International Journal of Thermofluid Science and Technology (2021)
Volume 8, Issue 2, Paper No. 080204
https://doi.org/10.36963/IJTST.2021080204
Research Article

Free convective heat transmission under LTNE in nanofluids within a trapezoidal permeable crater in view of three energy equations: influences of variable permeability and porosity

Sheikha M. Al-Waheibi[1], M. M. Rahman[1,*], M. Ziad Saghir[2]

[1]*Department of Mathematics, College of Science, Sultan Qaboos University, PO Box 36, PC 123 Al-Khod, Muscat, Sultanate of Oman*
[2]*Department of Mechanical and Industrial Engineering, Ryerson University, Toronto, Canada*

Received: 19 January 2021; Received in revised form: 05 March 2021; Accepted: 22 April 2021; Published online 19 May 2021

Abstract

Current research examines the effects of variable permeability and porosity through the free convective heat transmission flow of copper-water, aluminum oxide-water, and cobalt-water nanofluids via a glass bead permeable matrix within a trapezoidal crater in view of thermal non-equilibrium conditions amongst the permeable medium, nanoparticles, and the base fluid (three energy equations model). We employed the weighted residual Galerkin finite element strategy to simulate the non-dimensional model equations. We compared our results with the existing data from the open literature for a special case, and we get an excellent agreement with nominal relative error. We analyzed the influences of varying penetrability and porosity factors for different Nusselt numbers of fluid, nanoparticles, as well as the porous matrix in detail. The acquired numerical outcomes affirm that the critical Rayleigh number value to begin the thermal non-equilibrium situation diminished by expanding the glass bead diameter and the porosity parameter. Moreover, the expansion of variable porosity substantially amplifies the amount of heat transmission in a base fluid (approx. 120%) and nanoparticles (approx. 30%). The corresponding intensifications in Nusselt number of the base fluid, nanoparticles, and permeable medium are 100.7%, 6.3%, and 32.6%, respectively, when beads diameter increases from 0.1 to 0.4 for the Rayleigh number equal to 10^5. The interface heat transmission parameters (or Nield numbers) have an active part in controlling the heat transmission in different phases. Comparing with the other two nanofluids, we noticed that the base fluid, nanoparticles, and permeable matrix heat transmission coefficients are the highest in a copper-water nanofluid.

Keywords: Free convection, Nanofluids, permeability, Thermal non-equilibrium condition, Trapezoidal crater

**Corresponding e-mail*: mansurdu@yahoo.com; mansur@squ.edu.om (M. M. Rahman)

Nomenclature

A_1	aspect ratio	(U,V)	non-dimensional velocity components
A_2	aspect ratio	(x,y)	dimensional coordinates
c_1	empirical constant	(X,Y)	non-dimensional coordinates
c_2	empirical constant	Greek Symbols	
C_p	specific heat	α	thermal diffusivity
Da	Darcy number	β	factor of volume expansion
d_p	solid particles diameter inside the permeable matrix	γ	angle between inclined wall and y -axis
D_p	non-dimensional solid particles diameter	δ , δ_1, δ_2	conductivities-ratios
g	acceleration by the gravity	τ	nondimensional time
h_{fp}	interface heat transmission factor amid the base fluid and nanoparticles	ρ	fluid density
h_{fs}	interface heat transmission factor amid the base fluid and permeable medium	μ	dynamic viscosity
H	height of the enclosure	υ	kinematic factor of viscosity
K	permeability	θ	non-dimensional temperature
l	crater's top side length	ϕ	nano-particle loading
L	crater's bottom side length	κ	thermal conductivity
Ni	Nield number	λ	diffusivities-ratio
Ni_p	Nield number of the base fluid/nanoparticle interface	ε , ε^*	porosity
Ni_s	Nield number of the base fluid/permeable medium interface	ε_∞	uniform porosity
Nu	Nusselt number	(η, ξ)	coordinates along and normal to the inclined wall
p	dimensional pressure	Superscripts	
P	non-dimensional pressure	/	partial derivative w.r.t t , τ
Ra	Rayleigh number	Subscripts	
Ra_c	critical Rayleigh number	nf	nanofluid
S	non-dimensional length of the inclined wall	f	base fluid
t	dimensional time	p	solid particles
T	temperature	s	solid matrix
T_0	reference temperature	x , X	partial derivative w.r.t x , X
T_h	crater's hot side temperature	y , Y	partial derivative w.r.t y , Y
T_c	crater's cold side temperature	h	hot
(u,v)	dimensional velocity components	c	cold

1. Introduction

Recently, convection heat transmission in different cavities has pulled-in the consideration of numerous scientists. Because of its industrial significance, convective heat transmission inside various enclosures has enticed many kinds of research in this field. Thus, different issues identified with the convection heat transmission inside the cavities have been examined [1–3]. Nanofluids exhibit sensible usages in endless zones of industry, science, engineering, and numerous different spaces. Because of these practical uses, many researchers conducted the initial examinations to assess nanofluid heat transfer in various cavities by the disparate flow and diverse thermal circumstances [4–14]. Furthermore, nanofluids exhibit some noteworthy features that are varied from the usual colloidal suspensions. Experiments demonstrated that the physical physiognomies of regular fluid include thermal conductivity, density, and viscosity augment with the addition of nanoparticles [15- 16].

Convective heat transmission through the porous medium within an enclosure is a hot area of research that has numerous engineering and developed uses, for instance, thermal energy pipes, solar energy storage, dryers, computer chips, and insulation systems. Nield and Bejan [17] have conducted extensive reviews on nanofluid flows inside permeable matrixes. Kasaeian *et al.* [18] examined the progress within the region of thermal energy transmission and nanofluid flow through a permeable matrix by the arrangement of an extensive review. Throughout the years, numerous researches deal with natural convection heat transmission through a penetrable matrix [19-27]. However, a significant number of these investigations used the local thermal equilibrium (LTE) model amid nanofluid and permeable matrix. Basak *et al.* [28], Chamkha and Ismael [29], and Nield [30] used the model of LTE to study various characteristics of convective flow and heat transmission inside a permeable matrix. In LTE, the difference in temperature among the fluid and the permeable medium is insignificant. In many situations like textile transportation (Ye *et al.* [31]) and stellar atmospheres (Straughan [32]) where local thermal nonequilibrium (LTNE) phenomenon happens. Several studies of the LTNE model for fluid flow and heat transmission through the permeable matrix are reported ([33-42]). Arasteh *et al.* [43] examined nanofluid flow and thermal energy transmission through metal foam through a double-layered sinusoidal heat slash considering LTNE condition. They determined the performance evaluation criteria against the Darcy number, Reynolds number, and nanoparticle loading. The nanofluid flow through a porous enclosure is analyzed by Sheikholeslami and Shehzad [44] using the model of two temperatures. They found an inverse association between the permeability and the temperature slope. Astanina *et al.* [45] studied numerically free convection inside a square partially permeable crater by conducting heat source considering the LTNE model. They discovered that for LTNE, the total average Nusselt number rises with the intensification of the interface heat transmission coefficient and the permeable layer thickness.

Al-Weheibi and Rahman [46] analyzed thermal energy transmission in a penetrable trapezoidal cavity occupied by nanofluids utilizing the LTNE model. They established that the numbers of Darcy and Nield substantially regulate heat exchange amid nanofluid and solid phases. Sheremet *et al.* [47] directed numerical research on heat transmission inside a porous square crater considering two temperatures model and the Tiwari and Das model [48]. They confirmed that the raised loading of nanoparticles curbs the flow of nanofluid. Izadi *et al.* [49] considered the LTNE model and studied the natural convection flow through a permeable crater revealed to a non-uniform magnetic domain. They noted that because the

Hartmann number acts on the intensification of heat transmission in hybrid nanofluid, the application of the LTE is defensible. Ghalambaz *et al.* [50] analyzed the conjugate natural convection heat transmission inside a crater occupied by a permeable matrix utilizing LTNE effects. They observed that the maximum total amount of heat transmission relates to the situation where the elements are in the middle of the hot walls. Sabour and Ghalambaz [51] examined LTNE natural convection heat transmission of nanofluids through a triangular crater occupied by a permeable matrix considering a three energy equation and Buongiorno model. They noticed that expanding the factor of buoyancy ratio lessens and increment the rate of heat transmission in fluid and permeable phases, separately. Pop *et al.* [52] further investigated nanofluid flow in a permeable square crater utilizing LTNE and Buongiorno models. In their research, the Darcy model was utilized for the fluid flow and three energy equations for heat transfer. They reported that the average Nusselt number for nanoparticles rises, whereas it declines for fluid with the increments of the nanoparticles-fluid interface heat transmission factor.

The uniform porosity is regularly not proper in numerous utilizations, for example, pressed bed exchangers and settled bed catalytic gadgets. Recently, Al-Weheibi *et al.* [53] investigated the effects of variable porosity and permeability on the thermal intensification of Cu-H_2O nanofluid inside a trapezoidal cavity utilizing the model of LTNE. They noted that the critical Rayleigh number deciding the LTNE condition augmented by expanding the Nield number diminishes with the intensification of the diameter of the beads creating the permeable matrix. Abelman *et al.* [54] examined the heat transfer of a nanofluid saturated penetrable canal using flexible permeability. They reported that augmenting either the pressure gradient factor or the nanoparticle loading enhanced the thermal energy transmission.

The examination for the above literature suggests that an investigation is required to know the conditions for thermal exchange among the base fluid, nanoparticles, and the solid matrix having flexible permeability and variable porosity utilizing three energy equations in a right trapezoidal cavity. Consequently, we intended to explore the importance of varied penetrability and porosity on the time-dependent buoyancy prompted nanofluid (Cu-H_2O, Al_2O_3-H_2O, and Co-H_2O) flow in a right trapezoidal crater on account of LTNE state among the permeable medium, base fluid, and the nanoparticles considering Tiwari and Das nanofluid model together with Darcy-Brinkman model for the porous matrix. The gained mathematical outcomes provide information that could be useful in the improvement of a passive method of cooling for electric equipment as well as for advancing the structure of a solar hoarder in optimizing thermal harvesting. The rest of the current research is structured as follows: sect. 2 discusses the physical and mathematical models, whereas sect. 3 describes the solution technique. In sect. 4, we discussed the simulated results from physical and engineering viewpoints. Section 5 documents the significant outcomes of this study.

2. Formulation of the problem

We consider a laminar, two dimensional, time dependent buoyancy induced flow of different nanofluids inside a trapezoidal crater occupied by a permeable matrix having varying porosity and permeability. Figure 1 shows geometry, thermal conditions as well as flow structure. Gravity acts downwards. The lengths for the bottom, top, and vertical sides of the crater are L, $l(<L)$, and H, correspondingly with aspect ratios $A_1 = l/L = 0.5$ and $A_2 = H/L = 1$. The slanting side of the crater is maintained at the high temperature T_h and

the vertical side of the crater is subject to a uniform lower temperature T_c such that ($T_h > T_c$). We kept the bottom and top walls adiabatic. Moreover, it was assumed that there are no flow slips through the rigid margins. The LTNE condition is considered amid nanoparticles, base fluids, and porous medium. That is, we need to consider a three-energy equation model for temperature distributions. In the current study, for laminar flow where viscosity is the dominating dissipative factor, viscous dissipation and thermal radiation are presuming weak, so ignored.

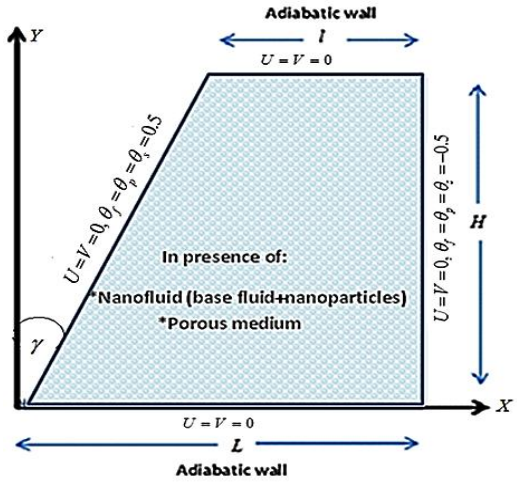

Fig. 1 The physical model with boundary conditions

Contingent on the previously stated assumptions and the Darcy-Brinkman Boussinesq model (Brinkman [55, 56]); the dimensional equations governing the present research are as described in the following: (Sheremet *et al.* [47], Tiwari and Das [48], Al-Weheibi *et al.* [53]):

$$u_x + v_y = 0 \tag{1}$$

$$0 = -p_x - \frac{\mu_{nf}}{K}u + \tilde{\mu}_{nf}\left(u_{xx} + u_{yy}\right) \tag{2}$$

$$0 = -p_y - \frac{\mu_{nf}}{K}v + \tilde{\mu}_{nf}\left(v_{xx} + v_{yy}\right) + (\rho\beta)_{nf}\, g(T_f - T_0) \tag{3}$$

$$T_f' + \frac{1}{\varepsilon}\left(u(T_f)_x + v(T_f)_y\right) = \frac{k_f}{(\rho C_p)_f}\left((T_f)_{xx} + (T_f)_{yy}\right) + \frac{h_{fs}}{\varepsilon(\rho C_p)_f}(T_s - T_f) + \frac{h_{fp}}{\varepsilon(\rho C_p)_f}(T_p - T_f) \tag{4}$$

$$T_p' + \frac{1}{\varepsilon}\left(u(T_p)_x + v(T_p)_y\right) = \frac{k_p}{(\rho C_p)_p}\left((T_p)_{xx} + (T_p)_{yy}\right) + \frac{h_{fp}}{\varepsilon(\rho C_p)_p}(T_f - T_p) \tag{5}$$

$$T_s' = \frac{k_s}{(\rho C_p)_s}\left((T_s)_{xx} + (T_s)_{yy}\right) + \frac{h_{fs}}{(1-\varepsilon)(\rho C_p)_s}(T_f - T_s) \tag{6}$$

Here, $T_0 = (T_c + T_h)/2$ is the reference temperature and prime indicates derivative with respect to t. The explanations of the rest of the factors are specified in the nomenclature. The

efficient dynamic viscosity of nanofluid $\tilde{\mu}_{nf}$ inside a porous matrix (Ochoa-Tapia and Whitaker [57]) is stated by $\tilde{\mu} = \frac{\mu_{nf}}{\varepsilon}$. The porosity ε varies on the perpendicular distance from the crater's bottom wall as follows (Chandrasekhara and Vortmeyer [58])

$$\varepsilon(y) = \varepsilon_{\infty}\left(1 + c_1 e^{\frac{-c_2 y}{d_p}}\right) \tag{7}$$

where empirical constants $c_1 = 1.4$ and $c_2 = 5$ (Hsu and Cheng [59]), d_p is the glass bead diameter creating the porous matrix, y is the minimum distance between the bead and the horizontal carter's side, ε_{∞} is the constant porosity. The permeability K of the porous matrix varies with the perpendicular distance from the bottom side of the crater as follows (Ergun [60])

$$K(y) = \frac{\varepsilon^3 d_p^2}{150(1-\varepsilon)^2} \tag{8}$$

The accompanying thermophysical relations are employed in our present study. In nanofluid research these thermophysical relations are widely used and highly cited by a great number of researchers. Although there exists other relations but those are also specific model dependent.

$$\rho_{nf} = (1-\phi)\rho_{bf} + \phi\rho_{sp} \text{ (Tiwari and Das [48])} \tag{9}$$

$$\frac{\mu_{nf}}{\mu_{bf}} = \frac{1}{(1-\phi)^{2.5}} \text{ (Brinkman [61])} \tag{10}$$

$$\frac{k_{nf}}{k_{bf}} = \frac{k_{sp} + 2k_{bf} - 2(k_{bf} - k_{sp})\phi}{k_{sp} + 2k_{bf} + (k_{bf} - k_{sp})\phi} \text{ (Maxwell [62])} \tag{11}$$

$$(\rho Cp)_{nf} = (1-\phi)(\rho Cp)_{bf} + \phi(\rho Cp)_{sp} \text{ (Nield and Bejan [17])} \tag{12}$$

$$\alpha_{nf} = \frac{k_{nf}}{(\rho Cp)_{nf}} \tag{13}$$

$$(\rho\beta)_{nf} = (1-\phi)(\rho\beta)_{bf} + \phi(\rho\beta)_{sp} \tag{14}$$

Table 1 reported the efficient thermo physical characteristics of the nanofluids (Oztop and Abu-Nada [63]).

Table 1 Thermo physical characteristics of H_2O and Cu, Al_2O_3 and Co (Oztop and Abu-Nada [63]).

Thermo physical characteristics	C_p (J/kgK)	ρ (kg/m^3)	κ (W/mK)	μ (Pas)	$\beta\times10^{-5}$ $(1/K)$
H_2O	4179	997.1	0.613	0.001003	21
Cu	385	8933	401	-	1.67
Al_2O_3	765	3970	40	-	0.85
Co	420	8900	100	-	1.3

The initial and boundary conditions for the nanofluid flow and temperature are:

for $t \le 0$, $u = v = p = T_f = T_p = T_s = 0$ (15)

The boundary conditions as illustrated in fig. 1 when $t > 0$ are:

$u = v = 0,\ (T_f)_y = (T_p)_y = (T_s)_y = 0$ for $0 \le x \le L,\ y = 0$ (16)

$u = v = 0,\ (T_f)_y = (T_p)_y (T_s)_y = 0$ for $L - l \le x \le L,\ y = H$ (17)

$u = v = 0,\ T_f = T_p = T_s = T_h$ for $0 \le x \le L - l,\ y = \dfrac{H}{L-l}x$ (18)

$u = v = 0,\ T_f = T_p = T_s = T_c$ for $x = L, 0 \le y \le H$ (19)

The following transformations are implemented to make eqs. (1)-(6) non-dimensional

$$\left.\begin{aligned} &X = \frac{x}{L}, Y = \frac{y}{L}, U = \frac{u}{(\alpha_f / L)}, V = \frac{v}{(\alpha_f / L)}, \tau = \frac{t\alpha_f}{L^2}, \\ &P = \frac{pK}{\mu_f \alpha_f}, \theta_f = \frac{T_f - T_0}{T_h - T_c}, \theta_p = \frac{T_p - T_0}{T_h - T_c}, \theta_s = \frac{T_s - T_0}{T_h - T_c}, T_0 = \frac{T_h + T_c}{2} \end{aligned}\right\} \quad (20)$$

Utilizing (20), eqs. (1)-(6), become:

$$U_X + V_Y = 0 \quad (21)$$

$$0 = -P_X - \frac{\mu_{nf}}{\mu_f}U + \left(\frac{Da}{\varepsilon^*}\frac{\mu_{nf}}{\mu_f}\right)\left(U_{XX} + U_{YY}\right) \quad (22)$$

$$0 = -P_Y - \frac{\mu_{nf}}{\mu_f}V + \left(\frac{Da}{\varepsilon^*}\frac{\mu_{nf}}{\mu_f}\right)\left(V_{XX} + V_{YY}\right) + \frac{(\rho\beta)_{nf}}{(\rho\beta)_f} Da\,\mathrm{Ra}\,\theta_f \quad (23)$$

$$\varepsilon^* \theta_f' + U(\theta_f)_X + V(\theta_f)_Y = \varepsilon^*\left((\theta_f)_{XX} + (\theta_f)_{YY}\right) + Ni_s(\theta_s - \theta_f) + Ni_p(\theta_p - \theta_f) \quad (24)$$

$$\varepsilon^* \theta_p' + U(\theta_p)_X + V(\theta_p)_Y = \varepsilon^* \frac{\alpha_p}{\alpha_f}\left((\theta_p)_{XX} + (\theta_p)_{YY}\right) + Ni_p \frac{(\rho C_p)_f}{(\rho C_p)_p}(\theta_f - \theta_p) \quad (25)$$

$$\lambda\theta_s' = \left((\theta_s)_{XX} + (\theta_s)_{YY}\right) + \frac{1}{(1-\varepsilon^*)} Ni_s\ \delta(\theta_f - \theta_s) \quad (26)$$

where $\varepsilon^*(Y)=\varepsilon_\infty\left(1+c_1e^{\frac{-c_2Y}{D_p}}\right)$, $Da=\frac{K(y)}{L^2}=\frac{\varepsilon^{*3}D_p^2}{150(1-\varepsilon^*)^2}$, $D_p=\frac{d_p}{L}$, $Ra=\frac{g\beta_f\left(T_h-T_c\right)L^3}{\upsilon_f\alpha_f}$ is the Rayleigh number, $Ni_s=\frac{h_{fs}L^2}{\kappa_f}$ is the Nield number of the base fluid/permeable medium interface, $Ni_p=\frac{h_{fp}L^2}{\kappa_f}$ is the Nield number of the base fluid/nanoparticle interface, $\lambda=\frac{\alpha_f}{\alpha_s}$ is the diffusivities-ratio, and $\delta=\frac{\kappa_f}{\kappa_s}$ is the conductivities-ratio. Prime is the derivative referring to τ.

Utilizing (20), eqs. (16)-(19) become:

$$U=V=0,\ (\theta_f)_Y=(\theta_p)_Y=(\theta_s)_Y=0 \text{ for } 0\le X\le 1,\ Y=0 \tag{27}$$

$$U=V=0,\ (\theta_f)_Y=(\theta_p)_Y=(\theta_s)_Y=0 \text{ for } 1-A_1\le X\le 1,\ Y=A_2 \tag{28}$$

$$U=V=0,\ \theta_f=\theta_p=\theta_s=0.5 \text{ for } 0\le X\le 1-A_1,\ Y=\frac{A_2}{1-A_1}X \tag{29}$$

$$U=V=0,\ \theta_f=\theta_p=\theta_s=-0.5 \text{ for } X=1,\ 0\le Y\le A_2 \tag{30}$$

where $A_1=\frac{l}{L}$, $A_2=\frac{H}{L}$ are aspect ratios.

The local Nusselt number generally evaluates the amount of heat transmission from the heated side of crater to the fluid. It is defined by $Nu_L=\frac{hL}{k_f\Delta T}$ where the heat transmission coefficient h is defined by $h=-\kappa\frac{\partial T}{\partial\xi}=-\kappa\left(\cos\gamma\frac{\partial T}{\partial x}+\sin\gamma\frac{\partial T}{\partial y}\right)$, κ is the fluid thermal conductivity, η is the coordinate parallel to the inclined wall and ξ is normal to it ([64]). In dimensionless variables local Nusselt number becomes

$$Nu_L=-\left(\frac{\kappa}{\kappa_f}\right)\left(\cos\gamma\frac{\partial\theta}{\partial X}+\sin\gamma\frac{\partial\theta}{\partial Y}\right) \tag{31}$$

Along the inclined heated wall of the crater ($X=\frac{1-A_1}{A_2}Y$), the average Nusselt number is defined as follows:

$$\overline{Nu}=\frac{1}{S}\int_0^S Nu_L\big|_{X=IW}\,dS \tag{32}$$

where $S=\frac{A_2}{\cos\gamma}$ is the nondimensional length of the inclined side of the crater, dS is the lesser element length alongside the inclined side of the crater and $IW=\frac{1-A_1}{A_2}Y$.

The average Nusselt numbers ($\overline{Nu_f}$), ($\overline{Nu_p}$), and ($\overline{Nu_s}$) corresponding to the base fluid ($\kappa = k_f$), nanoparticles ($\kappa = k_s$), and solid matrix ($\kappa = k_s$) along the inclined hot wall following (30) become:

$$\overline{Nu_f} = -\frac{1}{S}\int_0^S \left(\cos\gamma \frac{\partial \theta_f}{\partial X} + \sin\gamma \frac{\partial \theta_f}{\partial Y} \right)\Bigg|_{X=IW} dS \tag{33}$$

$$\overline{Nu_p} = -\frac{\delta_1}{S}\int_0^S \left(\cos\gamma \frac{\partial \theta_p}{\partial X} + \sin\gamma \frac{\partial \theta_p}{\partial Y} \right)\Bigg|_{X=IW} dS \tag{34}$$

$$\overline{Nu_s} = -\frac{\delta_2}{S}\int_0^S \left(\cos\gamma \frac{\partial \theta_s}{\partial X} + \sin\gamma \frac{\partial \theta_s}{\partial Y} \right)\Bigg|_{X=IW} dS \tag{35}$$

where, $\delta_1 = \frac{\kappa_p}{\kappa_f}$ and $\delta_2 = \frac{\kappa_s}{\kappa_f}$.

The total Nusselt number for all phases can be calculated as ([39, 45])

$$\overline{Nu_{fps}} = \varepsilon^*(\overline{Nu_f} + \overline{Nu_p}) + (1-\varepsilon^*)\overline{Nu_s} \tag{36}$$

3. Solutions method

We simulated the non-dimensional model eqs. (21)–(26) together with boundary conditions (27)–(30) using the commercial software COMSOL Multiphysics that utilizes the Galerkin weighted residual finite element method (FEM). This methodology is analyzed in-depth to solve heat transmission in nanofluid flows in a cavity by Al-Kalbani *et al.* [65], Uddin and Rahman [66], and Zienkiewicz and Taylor [67]. Creating the grid and testing the grid sensitivity for the solution is crucial in FEM usages. Besides, it's reasonable to equate the simulated outcomes by the accessible available reported mathematical/ experimental data for the approval of them.

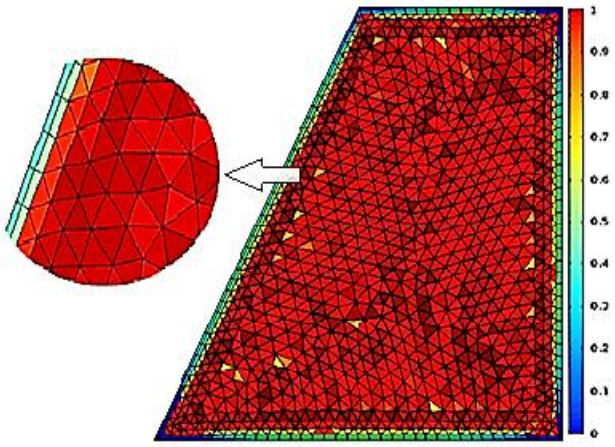

Fig. 2 Cavity mesh creation with zoom-in on a part of the cavity

In FEM, creating appropriate meshes is required for solving the boundary value problems successfully. It needs to evaluate the factors for example velocity, pressure, and

temperature on the generated networks. Figure 2 shows the generated meshes within the flow domain along with their quality measure.

We carried out simulation using glass bead as porous matrix and Cu-H_2O as nanofluid to assess the grid independency of the solution when $Ni_p = 10$, $Ni_s = 10$ $\phi = 0.05$, $\varepsilon_\infty = 0.8$, $D_p = 0.4$, $Ra = 10^5$, $A_1 = 0.5$, $A_2 = 1$, and $\tau = 1$. To acquire grid independent solutions, we examined five distinct meshes (normal, fine, finer, extra fine, and extremely fine) with 1241, 1988, 5547, 14610 and 20954 elements. Table 2 (and thereafter) represents the average Nusselt number ($Nu_f = S\overline{Nu_f}$, $Nu_p = (S/\delta_1)\overline{Nu_p}$, and $Nu_s = (S/\delta_2)\overline{Nu_s}$) established from the mathematical examination on the heated slanted side of the crater of the before stated elements for checking the mesh rigor. Table 2 shows that values of Nu_f , Nu_p, and Nu_s of 14610 mesh elements, when compared with 20954 mesh elements, indicate a high precision showing relative errors 3.39×10^{-4} %, 2.24×10^{-6} %, and 0 % respectively. Thus, the use of 14610 mesh elements is sufficient to produce numerical data with the aforesaid-precision, as well as saving computational time.

Table 2 Mesh sensitivity test of Cu-H_2O and Glass beads porous matrix at $Ni_p = 10$, $Ni_s = 10$, $\phi = 0.05$, $\varepsilon_\infty = 0.8$, $D_p = 0.4$, $Ra = 10^5$, $A_1 = 0.5$, $A_2 = 1$, and $\tau = 1$.

Elements number	1241	1988	5547	14610	20954
Nu_f	2.90055	2.90217	2.90424	2.94739	2.9474
Nu_p	893.10113	893.10255	893.10367	893.14486	893.14488
Nu_s	1.92874	1.92933	1.93125	1.93363	1.93363

Sheremet *et al.* [47] considered natural convective Cu-H_2O nanofluid flow within a square crater loaded up with consistent porosity aluminum foam permeable medium considering hot near wall, cold vertical wall, and bottom and top insulated walls. We compared our study with Sheremet et al. [47] in order to support the present numerical results for the parameter values $Ra = 10^3$, $\phi = 0.05$, $\varepsilon = 0.9$, and $Ni = 100$ utilizing two energy equations. The examination of Nu_{nf} and Nu_s presented in Table 3 shows a decent concurrence with this work. The relative error $\left|\frac{[47] - \text{present}}{[47]}\right| \times 100\%$ for Nu_{nf} is 1.8% whereas for Nu_s is 0.19%. This endorsement enhances the guarantee of our simulated data using the pde solver COMSOL Multiphysics with MATLAB interface.

Table 3 Comparison for average Nusselt numbers Nu_{nf} and Nu_s among current outcomes and Sheremet *et al.* [47] at $Ra = 10^3$, $\phi = 0.05$, $\varepsilon = 0.9$, and $Ni = 100$.

Authors	Nu_{nf}	Relative errror (%) for Nu_{nf}	Nu_s	Relative errror (%) for Nu_s
Sheremet *et al.* [47]	8.241		1.1321	
Present work	8.396	1.8%	1.1343	0.19%

Because of the absence of the results in the open literature on our specific geometry, we further validate our simulated-outcomes with the published data for a square crater occupied by a permeable medium in the absence of nanoparticles and LTNE. The near-side of the crater is hot, whereas the vertical side of the crater is cold. The remaining bottom and top walls are kept insulated. There is strong agreement (relative error about 0.06%) in Table 4 among the current data and those obtained by Baytas and Pop [68]. The curvature of streamlines and isotherms for this case is also very similar but not displayed here due to brevity.

Table 4 The average Nusselt number Nu_f comparison for a square permeable crater with results from the literature at $Ra = 1000$.

Authors	Nu_f	Relative error (%)
Baytas and Pop [68]	14.060	0.06
Present work	14.052	

4. Examination of the results

The simulated outcomes are contemplated in subtleties and investigated to look at variable permeability and porosity influences taking into account the LTNE states for the natural convective heat transmission nanofluid flow in a right-trapezoidal crater in consideration of three heat equations model. The outcomes explained the impacts of the Rayleigh number (Ra), loading of nanoparticles (ϕ), diameter of bead (D_p), porosity factor (ε_∞) and the Nield numbers (Ni_p, Ni_s) on the rate of heat transmission of base fluid (Nu_f), nanoparticle (Nu_p), and solid matrix (Nu_s) together with the dispersion of temperature in base fluid (θ_f), nanoparticle (θ_p) and solid medium (θ_s) along the main diagonal $Y = X$ and the cut line $Y = 2X - 0.05$ in the vicinity of the hot slanted side of the crater. We utilized three diverse nanofluids and glass bead (GB) as a penetrable matrix for the numerical experiment. The default values for model factors are taken as $Ra = 10^5$, $D_p = 0.4$, $Ni_p = 10$, $Ni_s = 10$, $\varepsilon_\infty = 0.8$, $\phi = 0.05$ and $\tau = 1$ (that is steady-state) together with Cu-H_2O nanofluid and glass bead (GB) porous matrix unless otherwise indicated. The aspect ratios are kept constant as $A_1 = 0.5$ and $A_2 = 1$ throughout the calculations. The numerous factors impacts on the flow and thermal regions are uncovered distinctively using the factor domain $(10^3 \le Ra \le 10^5)$, $(5 \le Ni_p, Ni_s \le 20)$, $(0.1 \le D_p \le 0.8)$, $(0.2 \le \varepsilon_\infty \le 0.8)$, and $(0 \le \phi \le 0.1)$.

4.1. Key factors impact on LTNE states

Figures 3(a)-(b) illustrate the difference between LTNE and LTE conditions respectively through dimensionless temperatures θ_f, θ_p, and θ_s inside the crater alongside the line ($Y = 2X - 0.05$) utilizing Cu-H_2O nanofluid and GB permeable medium

whe $Ra = 10^5$, $D_p = 0.4$, $\phi = 0.05$, $Ni_p = 10$, $Ni_s = 10$, and $\tau = 1$ for $\varepsilon_\infty = 0.6$, 0.2 respectively. We found that for smaller porosity, the thermal states of the fluid, nanoparticles, in addition to the penetrable matrix reach in equilibrium, hence LTE is achieved. The critical Rayleigh number Ra_c upon which the condition varies from LTE (wherein the temperatures θ_f , θ_p, and θ_s alike) to LTNE (wherein the temperatures θ_f , θ_p, and θ_s differ) changing D_p and ε_∞ considering Cu-H_2O and GB porous medium is clarified in fig. 4. From this fig., it is apparent that the value of Ra_c reduces by expanding D_p and ε_∞, which indicates that the thermal condition will alter from LTE to LTNE more rapidly by incrementing D_p and ε_∞. Increasing glass bead diameter expands the void space within the porous medium, which eases the base fluid and nanoparticles to flow quickly as a consequence, the buoyancy force intensifies, and the system reaches in LTNE state with smaller Rayleigh number.

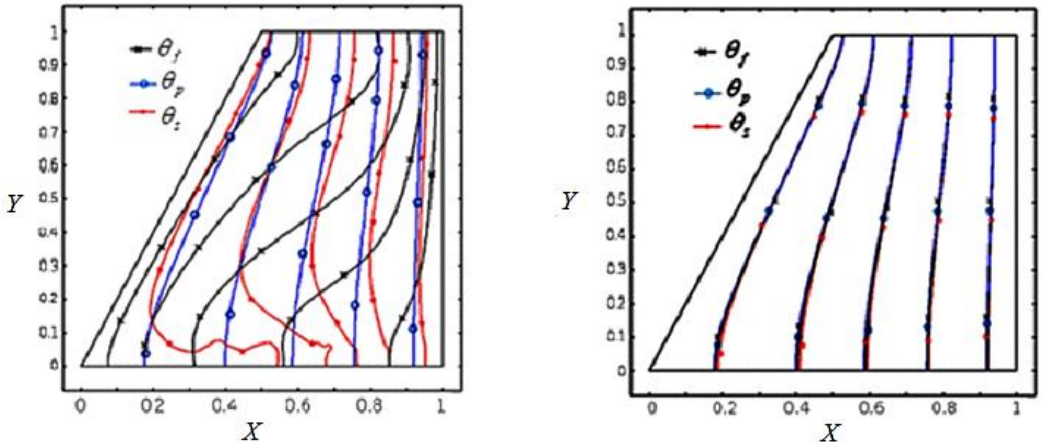

Fig. 3 Non-Dimensional temperature contours alongside the line $(Y = 2X - 0.05)$ utilizing Cu-H_2O and GB permeable medium when $Ra = 10^5$ $D_p = 0.4$, $\phi = 0.05$, $Ni_p = 10$, $Ni_s = 10$, and $\tau = 1$ for (a) $\varepsilon_\infty = 0.6$ and LTNE state, (b) $\varepsilon_\infty = 0.2$ and LTE state

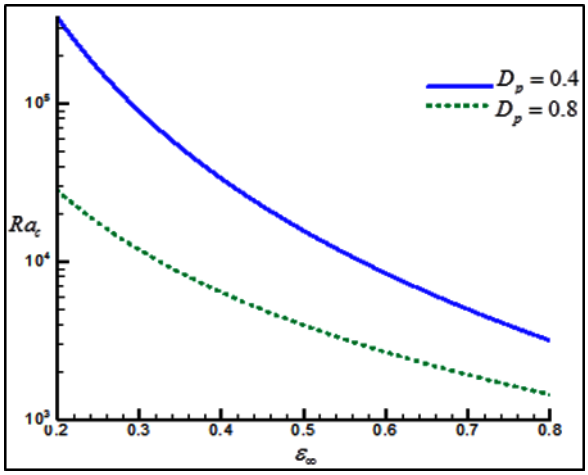

Fig. 4 Critical Rayleigh number Ra_c with various values of ε_∞ and D_p utilizing Cu-H_2O and GB permeable medium at $Ni_p = 10$, $Ni_s = 10$, $\phi = 0.05$ and $\tau = 1$

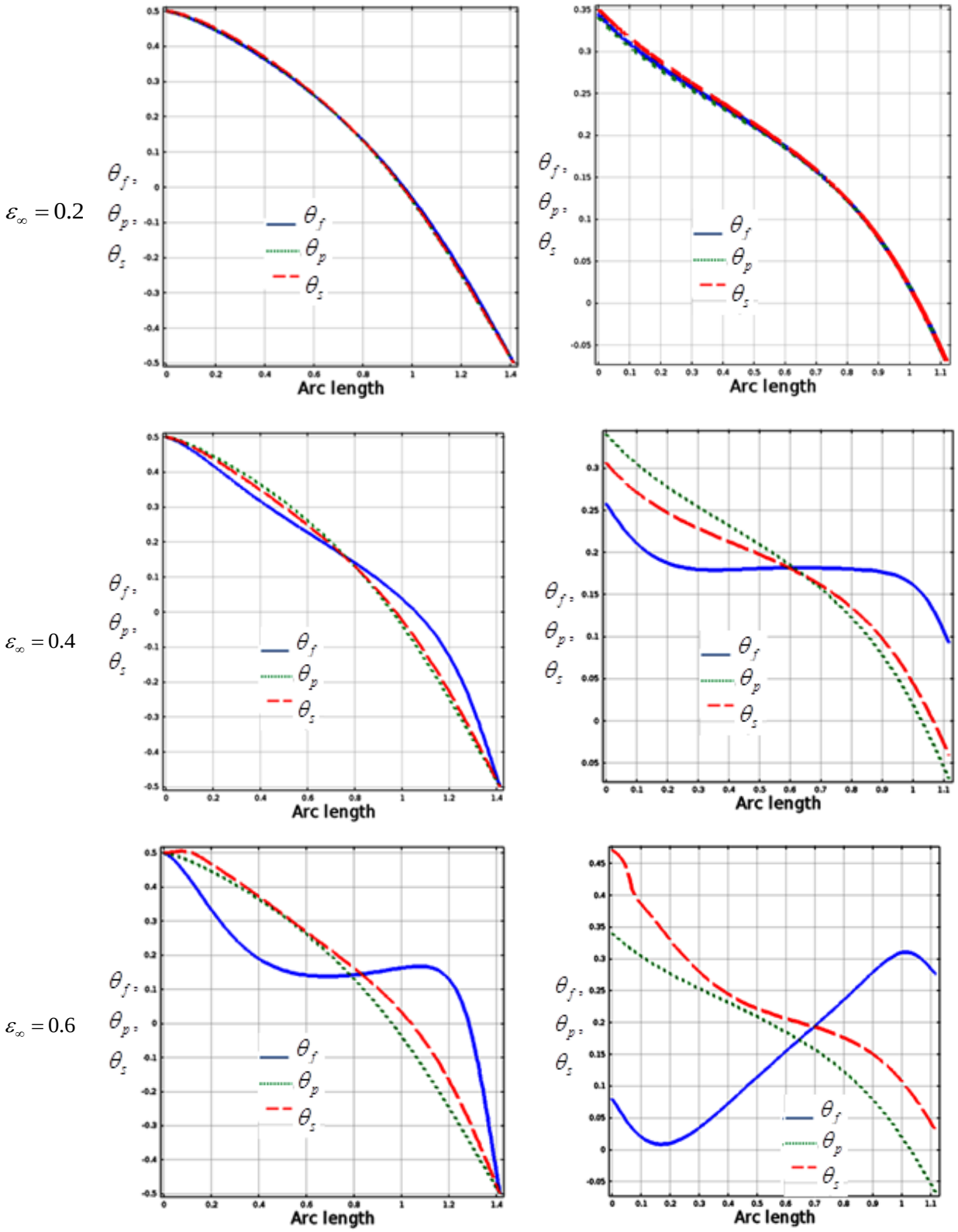

Fig. 5 Condition of LTE and LTNE via the non-dimensional temperature contours on the crater diagonal $(Y = X)$ (1^{st} column) and the line $(Y = 2X - 0.05)$ (2^{nd} column) with various values of ε_∞

As well it can be observed in fig. 5, the thermal condition alters from LTE to LTNE with the increase of ε_∞ through the lines $Y = X$ and $Y = 2X - 0.05$. We discovered in fig. 6 that Ni_p and Ni_s irrelevantly change the state from LTE to LTNE. Correspondingly, fig. 7 exhibits the effect of ϕ on the profiles of θ_f, θ_p, and θ_s through $Y = 2X - 0.05$. One can noted that ϕ inconsequentially modifies the condition of the permeable medium, base fluid, and nanoparticles from LTE to LTNE. Thus, the nanoparticle volume fraction impact in changing the state is negligible. Al-Weheibi and Rahman [46] studied a model having two-temperature equations and uniform porosity. They reported that Da and Ni are the primary factors that constrain the alteration of condition between LTE and LTNE. They further revealed that for $Da = \mathrm{O}(10^{-5})$ and regardless of Ni values, the porous medium and nanofluid become LTE states. Likewise, the system come to in LTE condition when $Ni = \mathrm{O}(10^5)$ irrespective of Da. Besides, the role of ε_∞ and ϕ on the state change amid the permeable matrix and the nanofluid are minimal. Constrained to the variable permeability and a two-heat equations model, Al-Weheibi *et al.* [53] confirmed that the critical Ra_c is increased with Ni and diminished with D_p and ε_∞.

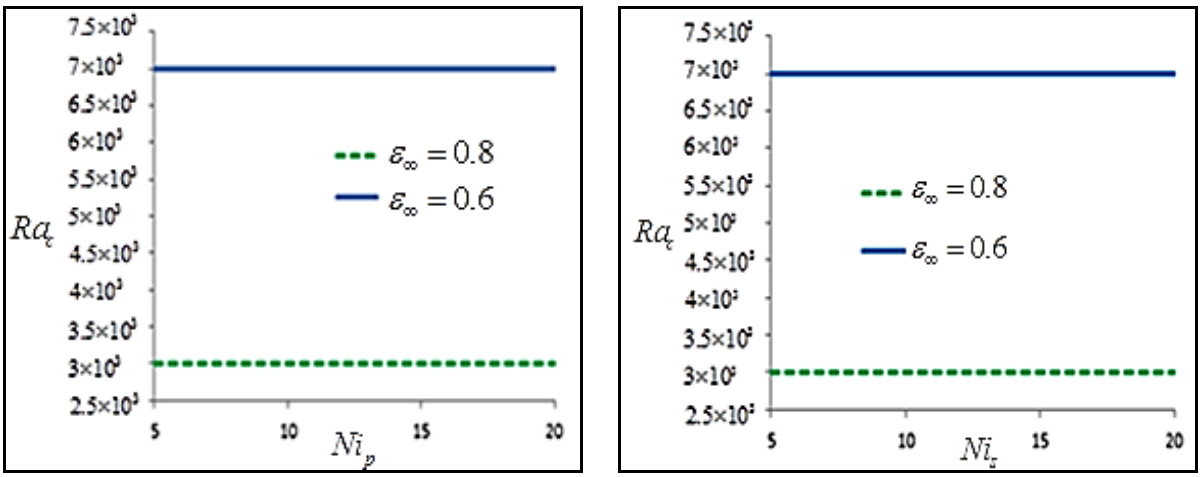

Fig. 6 Critical Rayleigh number Ra_c with various values of (a) Ni_p and ε_∞, (b) Ni_s and ε_∞ utilizing Cu-H_2O and GB porous medium when $D_p = 0.4$, $Ni_s = 10$, $\phi = 0.05$ and $\tau = 1$

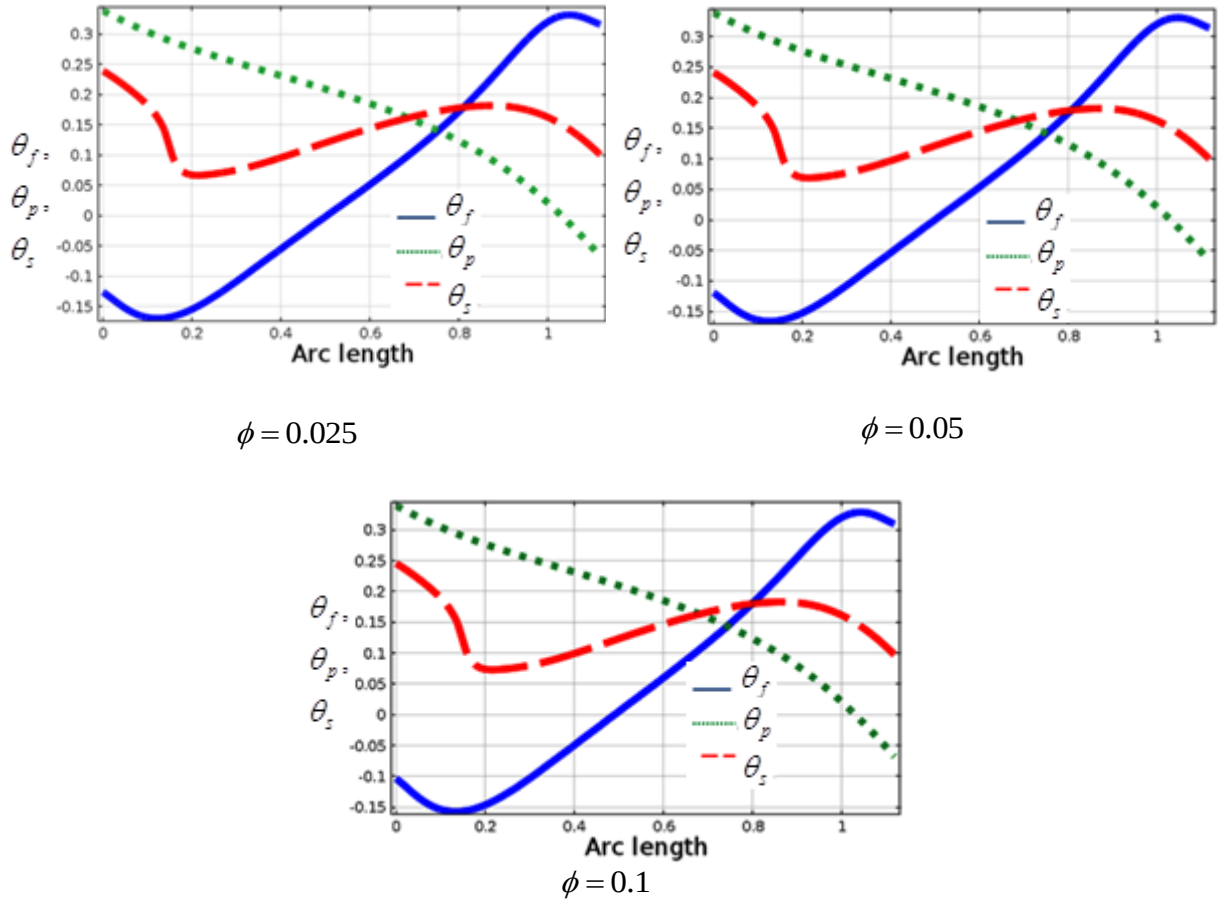

$\phi = 0.025$ $\phi = 0.05$ $\phi = 0.1$

Fig. 7 Temperature dispersion on the line $Y = 2X - 0.05$ utilizing Cu-H_2O with GB permeable medium for various values of ϕ when $Ra = 10^5$, $D_p = 0.4$, $\varepsilon_\infty = 0.8$, $Ni_p = 10$, $Ni_s = 10$ and $\tau = 1$

4.2. Thermal buoyancy parameter impact

An enhanced buoyancy force, hence an expansion of the thermal Rayleigh number, leads to more grounded convection in the flow region than conduction. Accordingly, the amplification of the convective flow in the crater and the boundary layers is becoming increasingly imperative. An intensification of Nu_f appears for Ra exceeding 10^4, which is clear in fig. 8(a). Along these lines, increasing the buoyancy force induces an augmentation of heat transfer rate. As well, in fig. 8(b) there is an intensification in Nu_p by incrementing Ra. Figures 9(a)-(c) elucidate the relationship amid Ra, Nu_f, Nu_p, and Nu_s for various kinds of nanofluids and glass bead (GB) porous matrices. We found that utilizing Cu-H_2O in contrast to Co-H_2O and Al_2O_3-H_2O leads to the uppermost rate of Nu_f, Nu_p, and Nu_s for numerous values of Ra. Figures 10(a)-(c) depicts that expanding Ra prompts expanding Nu_f, Nu_p, and Nu_s for various D_p values.

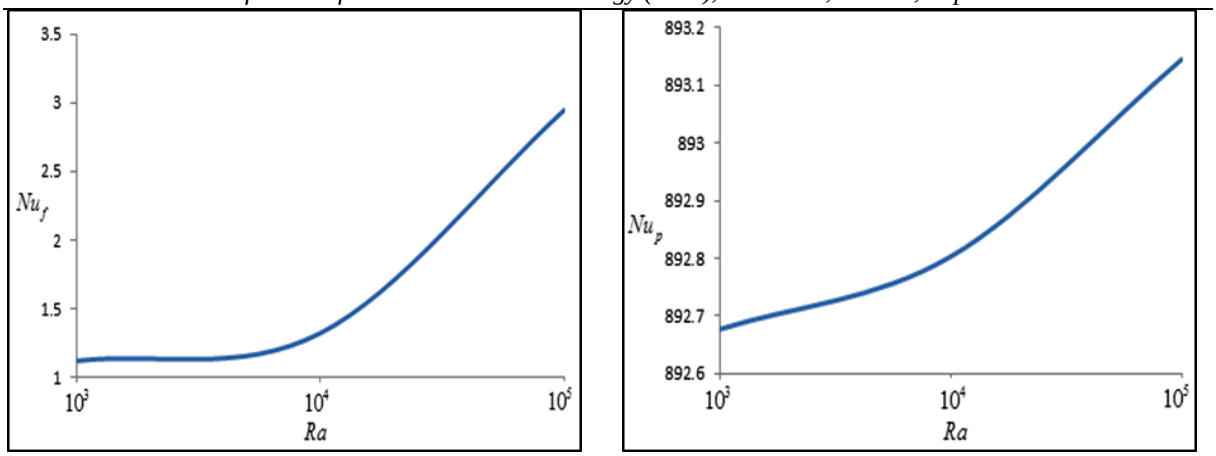

(a) (b)

Fig. 8 Average Nusselt number (a) Nu_f , and (b) Nu_p with various values of Ra utilizing Cu-H_2O and GB porous matrix at $\phi = 0.05$, $D_p = 0.4$, $\varepsilon_\infty = 0.8$, $Ni_p = 10$, $Ni_s = 10$ and $\tau = 1$

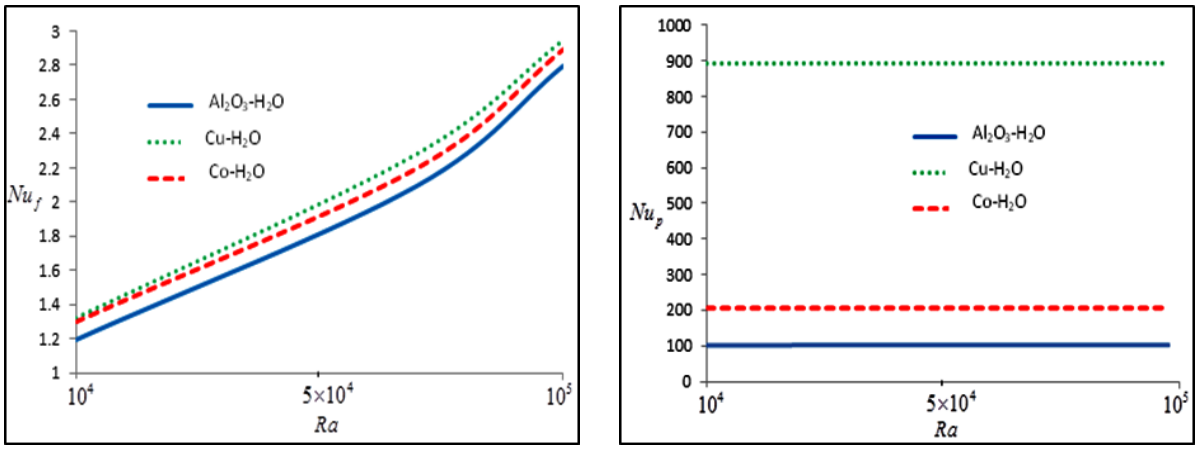

(a) (b)

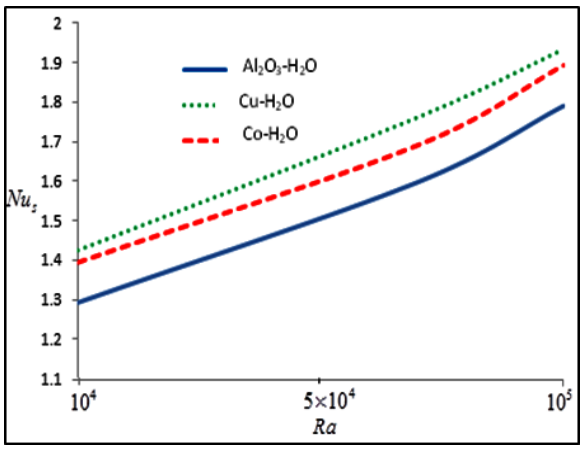

(c)

Fig. 9 Average Nusselt number (a) Nu_f , (b) Nu_p , (c) Nu_s with various values of Ra using numerous nanofluids and GB porous medium when $\phi = 0.05$, $D_p = 0.4$, $\varepsilon_\infty = 0.8$, $Ni_p = 10$, $Ni_s = 10$ and $\tau = 1$

4.3. Bead size creating the permeable medium impact

Figures 10(a)-(c) exhibit the variations of Nu_f, Nu_p, and Nu_s *vs* Ra for different values of D_p for Cu-H_2O nanofluid with glass bead permeable medium when $\phi = 0.05$, $Nip = Nis = 10$, $\varepsilon_\infty = 0.8$, and $\tau = 1$. We found that Nu_f, Nu_p, and Nu_s directly rises with D_p at a fixed Ra. At $Ra = 10^5$, the corresponding increases are 100.7%, 6.3%, and 32.6% when D_p increases from 0.1 to 0.4. Darcy number (Da) rises with D_p ; thus, the medium's permeability increases as well. Consequently, the rate of heat transmission got inflated. For a fixed D_p, the heat transmission variation in base fluid and the porous matrix is nonlinear, whereas it remains constant for the nanoparticles. Higher nonlinearity indicates stronger convection.

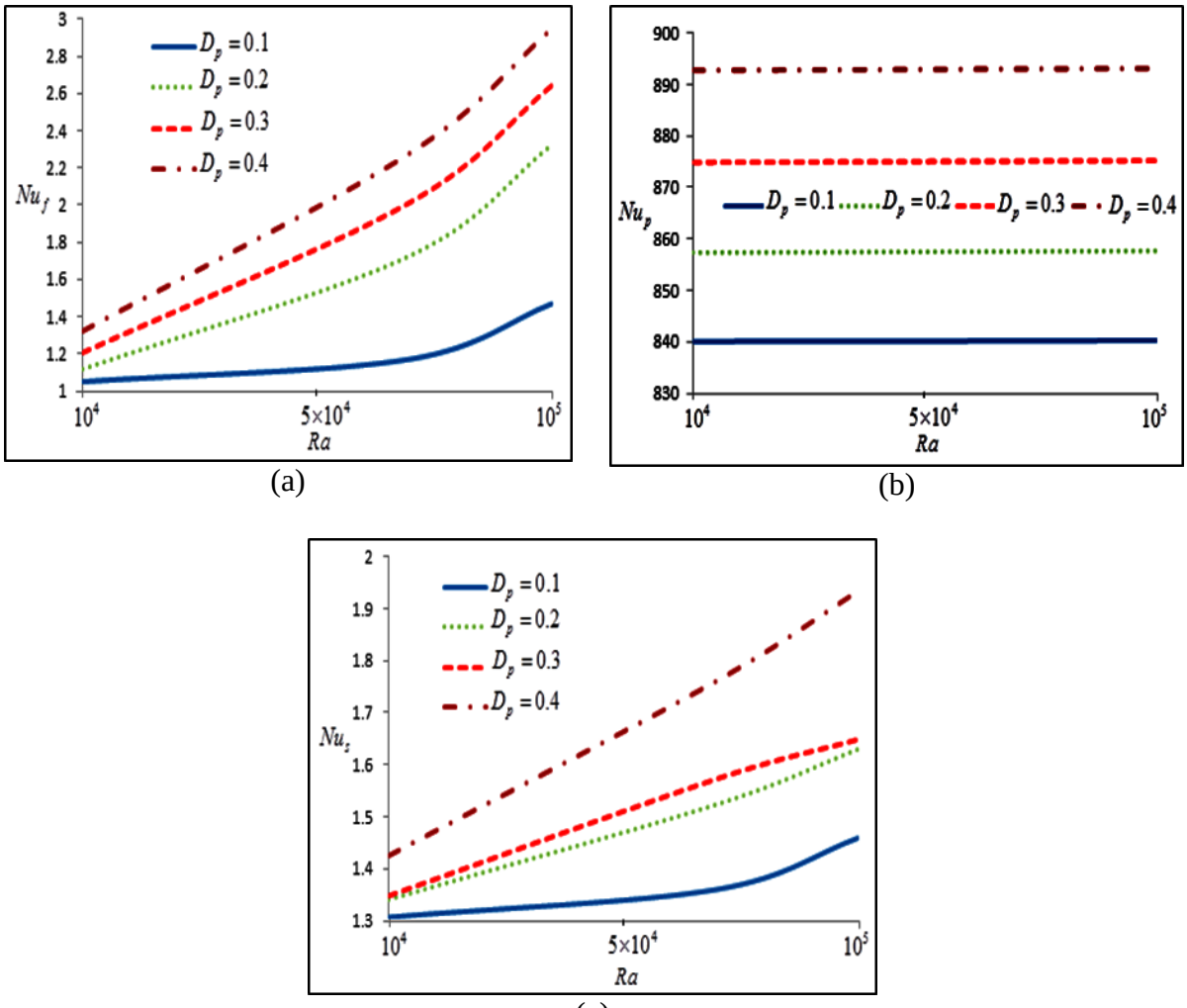

(a) (b)

(c)

Fig. 10 Average Nusselt number (a) Nu_f, (b) Nu_p, (c) Nu_s with various values of D_p and Ra utilizing Cu-H_2O with GB permeable medium at $Ni_p = 10$, $Ni_s = 10$, $\phi = 0.05$, $\varepsilon_\infty = 0.8$, and $\tau = 1$

4.4. Nield number impact

Figures 11(a)-(c) show the average Nusselt number Nu_f, Nu_p, and Nu_s against the Nield number Ni_p and Ni_s when $Ra = 10^5$, $D_p = 0.4$, $\varepsilon_\infty = 0.8$, and $\tau = 1$ varying ε_∞ utilizing the nanofluid (Cu-H_2O) and the porous matrix (glass bead). Figure 11a displays that the intensification of the interface factors (Ni_s & Ni_p) decreases the heat transmission of the fluid on the perpendicular side of the crater. Indeed, increasing the interface heat transmission factors diminishes the temperature variance amid the hot wall and the fluid, which eventually leads to reduce heat transmission rate on the fluid level. Figure 11b indicates that Nu_p increases with the intensification of Ni_p. The deterioration of the temperature variance among the fluid and the hot side of the crater implies the intensification of the fluid phase temperature near the inclined hot side of the crater with the association of nanoparticles. When the fluid temperature is lesser than the corresponding nanoparticles temperature, the hotter nanoparticles lose some of the heat to the fluid. Thus, nanoparticles temperature reduces, and accordingly, the temperature variance amongst nanoparticles and the heated side of the crater increments. Increasing the temperature variance among the nanoparticles and the heated inclined side of the crater leads to the expansion of the gradient of nanoparticles' temperature, which then intensifies Nu_p. Increasing interaction amid the permeable matrix and the base fluid increases the fluid temperature inside the region of the hot side of the crater. Therefore, the fluid phase temperature might be near or higher than the nanoparticles temperature; so, the fluid will ingest a little quantity of thermal energy from the nanoparticles or transfer a certain quantity of it to the nanoparticles. The outcomes of fig. 11(b) further display that by increasing Ni_s, the fluid phase will transfer a certain quantity of heat to the nanoparticles; thus, the nanoparticles temperature augmented. Consequently, the incline of temperature decreases so, Nu_p decreases with Ni_s.

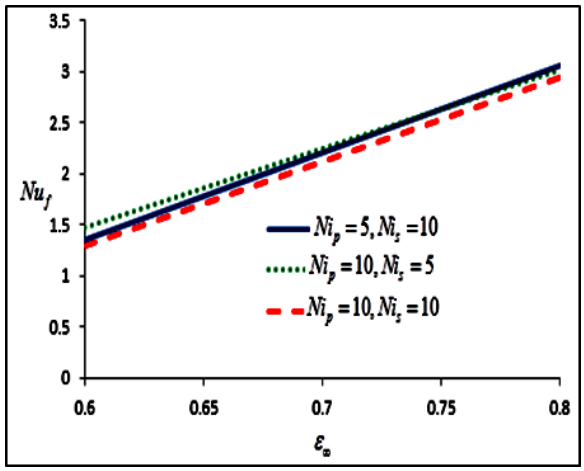

(a)

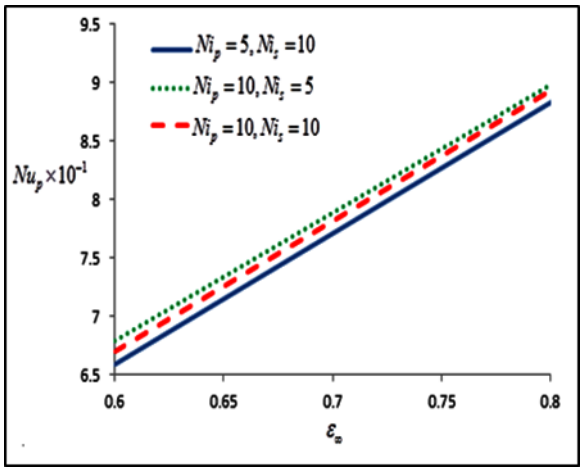

(b)

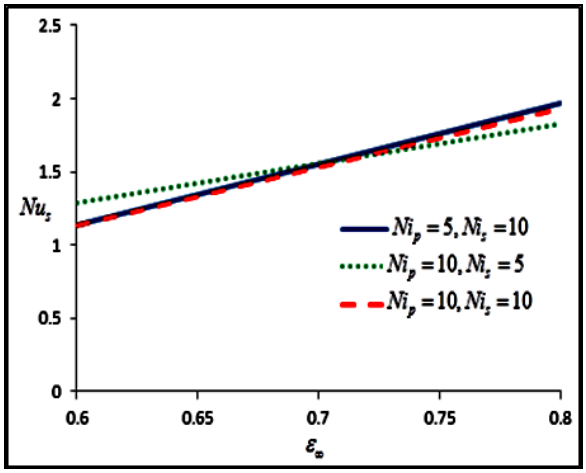

(c)

Fig. 11 Average Nusselt number (a) Nu_f, (b) Nu_p, (c) Nu_s with various values of Ni_p, Ni_s and ε_∞ utilizing Cu-H_2O with GB permeable medium at $D_p = 0.4$, $Ra = 10^5$, $\phi = 0.05$ and $\tau = 1$

Figure 11c displays the influence of interface heat transmission factors on the heat transmission rate of the permeable matrix. When $\varepsilon_\infty > 0.7$, the amplification of Ni_s considerably rises Nu_s. Since increasing Ni_s expands the thermal interaction among the base fluid and the permeable matrix, that leading to the intensification of the fluid temperature and concurrently the decrease of the porous phase temperature. Decreasing the permeable medium temperature, near the heated wall, accordingly will enhance Nu_s. When $\varepsilon_\infty < 0.7$, an opposite drift is observed. Lastly increasing Ni_p, slightly decreases Nu_s. Undoubtedly, increasing Ni_p raises the heat transmission interaction among the fluid and nanoparticles that leads to the intensification of the fluid temperature. So, the thermal energy absorbed by the fluid from the permeable medium declines. Thus, the temperature contrast among the wall and the permeable medium stays little, and therefore, the temperature enhancement in the permeable medium is little.

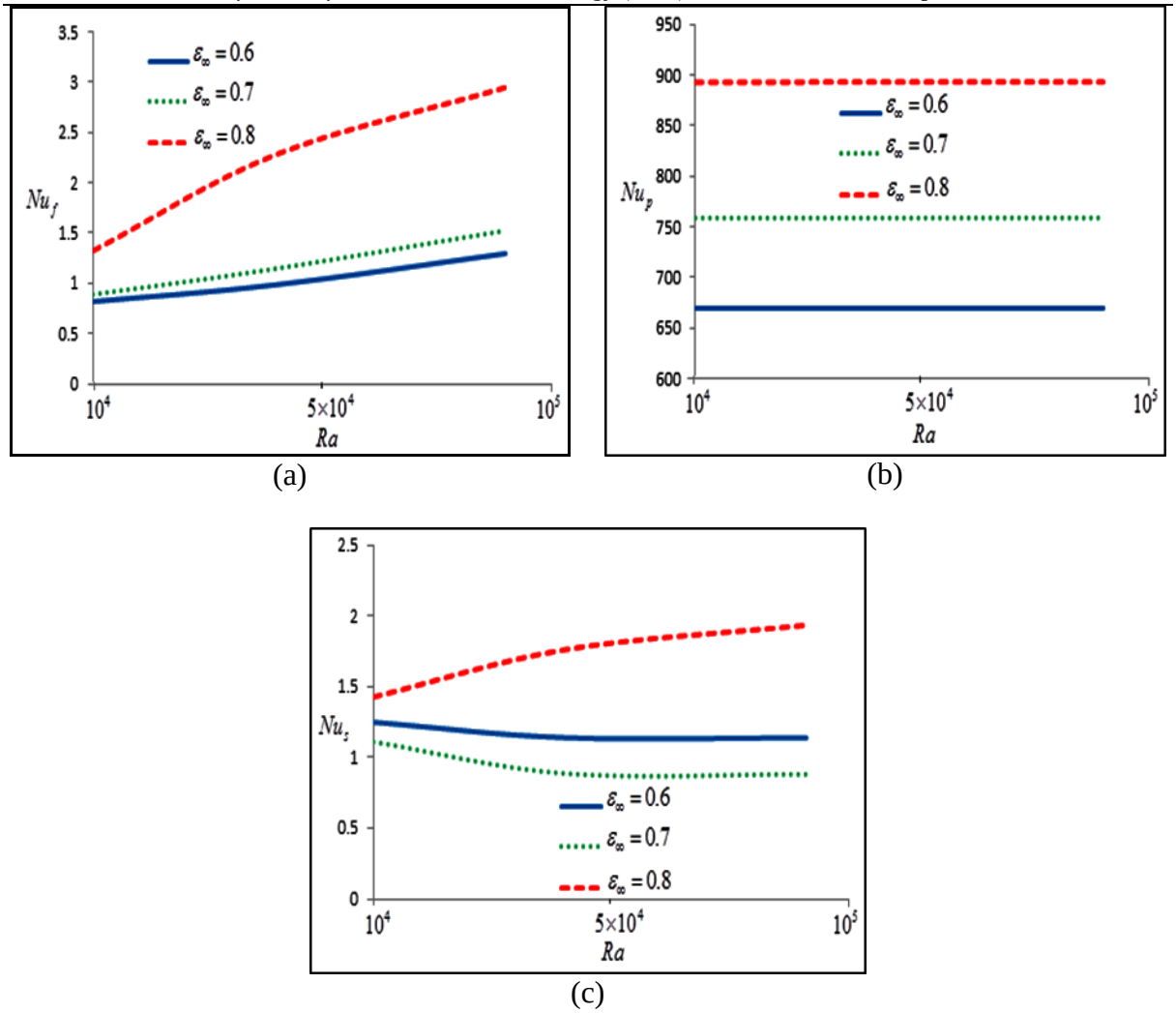

Fig. 12 Average Nusselt number (a) Nu_f, (b) Nu_p, (c) Nu_s with various values of ε_∞ and Ra utilizing Cu-H_2O with GB permeable medium at $Ni_p = 10$, $Ni_s = 10$, $D_p = 0.4$, $\phi = 0.05$ and $\tau = 1$

It is good to comment that, in our analysis, we have used the Nield number (Ni) instead of Sparrow number (Sp). The Sparrow number, defines $Sp = \frac{h_s L^2}{\kappa_e r_h}$ where h_s (W/m^2K) is the interfacial heat transmission factor, r_h (m) is the hydraulic diameter, and κ_e (W/mK) is the stagnant thermal conductivity of the permeable medium ([33]-[35]). It is represented by Nield number as $Ni_s = \frac{h_{fs} L^2}{\kappa_f}$ as $Sp = \frac{h_s L^2}{\kappa_e r_h} = \frac{h_{fs} L^2}{\kappa_f} \frac{k_f}{k_e} = Ni_s \left(\frac{k_f}{k_e} \right)$ considering $h_{fs} = \frac{h_s}{r_{rh}}$. Minkowycz *et al.* [33] pointed out that the local thermal equilibrium LTE exits when Sp is large. In our recent paper (Al-Weheibi [47]), we reported that LTE

exits when the Nield number is high that can be considered as a consequence of the increase of the Sparrow number.

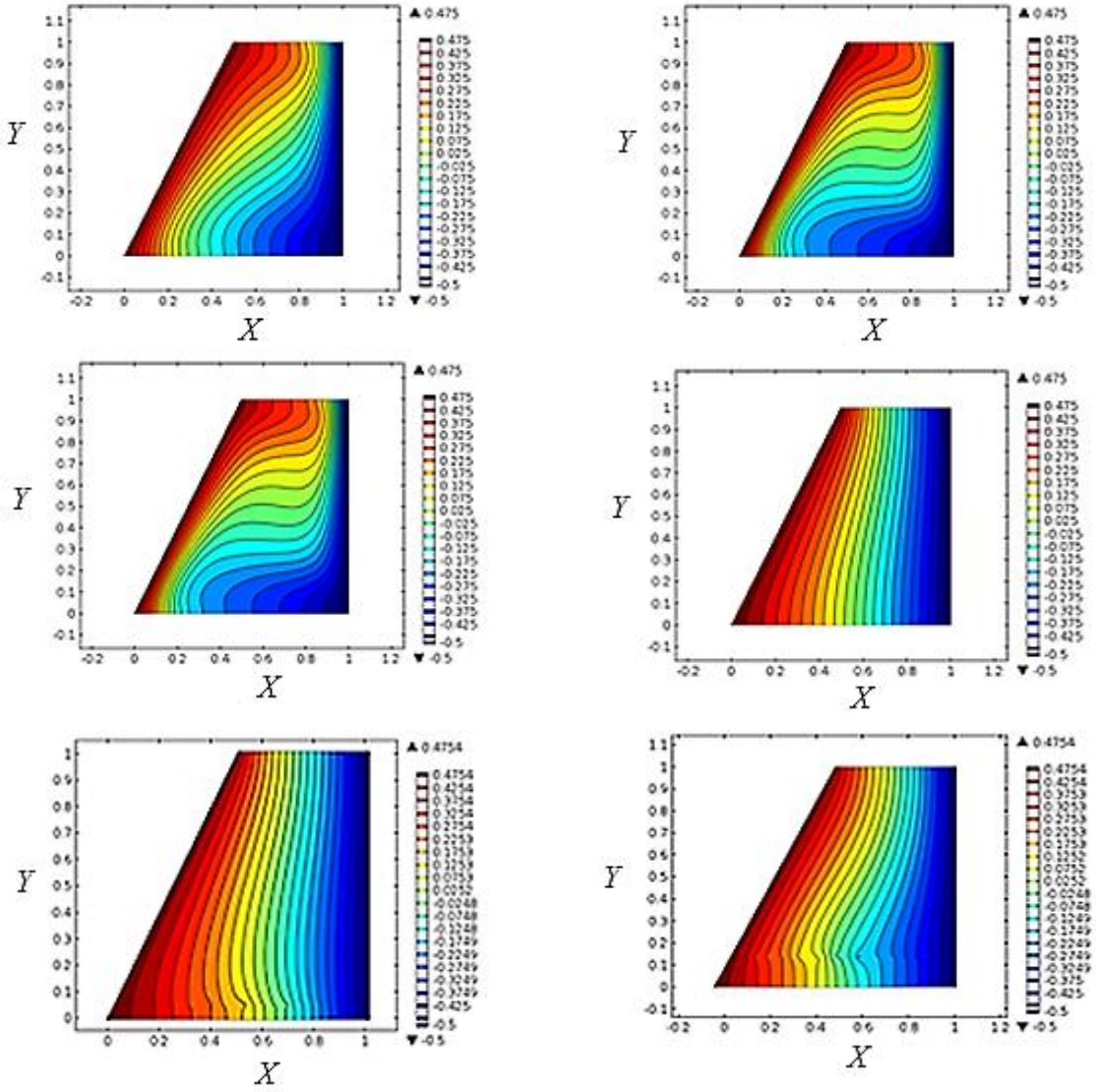

Fig. 13 Isotherms for θ_f (first row), θ_p (second row), and θ_s (third row) with different values of $\varepsilon_\infty = 0.6$ (1st column) and $\varepsilon_\infty = 0.8$ (2nd column) using Cu-H_2O and GB porous medium when $Ni_p = 10$, $Ni_s = 10$, $Ra = 10^5$, $\phi = 0.05$, $D_p = 0.4$, and $\tau = 1$

4.5. Porosity impact of the permeable medium

Figure 12(a) exhibits Nu_f with the Ra for numerous values of ε_∞. An increase in ε_∞ prods the expansion of Nu_f. The one can notice that the Nu_f increments for about 128% as ε_∞ increments from 0.6 to 0.8 when $Ra = 10^5$. As the permeable medium porosity expands, the volume of pores in the crater magnifies, which induces the augmentation in the

convective flow and the rate of the heat transfer inside the crater. Figure 12(b) displays the comparative perception of Nu_p. The value of Nu_p increments for approximately 33% as ε_∞ increases from 0.6 to 0.8 when $Ra = 10^5$. Figure 12(c) demonstrates that Nu_s fluctuates with the porosity parameter (ε_∞). For the smaller value of ε_∞, nanoparticles move slowly through the void space so, the heat carried by the nanoparticles is absorbed quickly by the solid matrix and behaves like a conduction mode of heat transfer in a solid body. A bigger void space allows the nanoparticles to move faster and carries more thermal energy from the heated side of the crater to the fluid before absorbed into the porous matrix; therefore, the heat transfer convection mode prevail.

Figure 13 shows the variations of isotherms for base-fluid, nanoparticles, and porous-matrix inside the enclosure against the porosity parameter. We found significant distortion of fluid isotherms (1st row) for the intensification of the porosity. It is due to the higher convection within the flow domain. The changes in nanoparticle isotherms (2nd row) are minimal for changes in ε_∞. Furthermore, solid-matrix isotherms bit fluctuates with the porosity varying. Moreover, we found that for large porosity ($\varepsilon_\infty \geq 0.6$), the isotherms of base-fluid, nanoparticles, and permeable-matrix are unlike indicates the system in LTNE state. For $\varepsilon_\infty < 0.6$, the system is tested and found in LTE state (not depicted here).

5. Conclusions

In the recent research, we examined the influences of varying porosity and varying permeability through the transient heat transfer of three different nanofluids (Cu-H_2O, Al_2O_3-H_2O, and Co-H_2O) flowing in a permeable medium (glass bead) in a trapezoidal crater employing LTNE condition amongst the nanoparticles, base fluid, and solid matrix. The non-dimensional temperature contours are depicted alongside the crater's main-diagonal ($Y = X$) and the line ($Y = 2X - 0.05$). Besides, we examined the effects of varying penetrability and varying porosity factors on the Nusselt numbers: Nu_f, Nu_p, and Nu_s in detail. The relative error is about 0.06% and 0.19% respectively when we compared our results with Baytas and Pop [68], and Sheremet *et al.* [47] for a special case. From the simulated data, we list the following major conclusions:

- The value of the critical Rayleigh number (Ra_c) for the onset of the LTNE state diminished by the expansion of the glass bead diameter (D_p) and the porosity parameter (ε_∞).
- The rate of heat transmission in base fluid (Nu_f), nanoparticles (Nu_p), and porous matrix (Nu_s) intensified with the increase of D_p. The corresponding intensifications are 100.7%, 6.3%, and 32.6%, respectively, when D_p increases from 0.1 to 0.4 at $Ra = 10^5$.
- The values of Nu_f and Nu_p increased by approximately 128% and 33%, respectively, when ε_∞ enlarged from 0.6 to 0.8 for $Ra = 10^5$.

- The rate of heat transfer in base fluid (Nu_f) decreases with the increase of the Nield numbers Ni_s and Ni_p.
- The average Nusselt number for nanoparticles (Nu_p) increased with Ni_p, whereas decreased with Ni_s.
- The average Nusselt number Nu_s declines smoothly by the intensification of Ni_p. For $\varepsilon_\infty > 0.7$, the value of Nu_s increases quite rapidly with Ni_s, whereas the scenario reverses when $\varepsilon_\infty < 0.7$.
- The average Nusselt numbers Nu_f, Nu_p, and Nu_s, are the highest for the Cu-H_2O nanofluid compared to the Co-H_2O and Al_2O_3-H_2O nanofluids.

Furthermore, it is crucial to enrich this study taking into consideration a full 3D model that we aim to communicate in our next study.

Declaration

Funding: Current research was financed by the research grants IG/SCI/MATH/20/03 and RC/RG-SCI/MATH/20/01

Conflict of Interest: The authors affirm that there is no conflict of interest.

Availability of data and material: Not applicable.

Code availability: Not applicable

References

[1] S. A. M. Mehryan, M. Ghalambaz, R. K. Feeoj, A. Hajjar, M. Izadi, Free convection in a trapezoidal enclosure divided by a flexible partition. Int J Heat Mass Transf. 149 (2020) 119186.
[2] A. Guha, A. Jain, K. Pradhan, Computation and physical explanation of the thermo-fluid-dynamics of natural convection around heated inclined plates with inclination varying from horizontal to vertical. Int J Heat Mass Transf. 135 (2019) 1130-1151.
[3] S. A. M. Mehryan, A. J. Chamkha, M. A. Ismael, M. Ghalambaz, Fluid–structure interaction analysis of free convection in an inclined square cavity partitioned by a flexible impermeable membrane with sinusoidal temperature heating. Meccanica. 52(11-12) (2017) 2685-2703.
[4] K. S. Al-Kalbani, M. M. Rahman, Convective heat transfer in the flow of a nanofluid in an inclined square enclosure. J Eng Phys Thermophy. 92(5) (2019) 1150-1170.
[5] L. M. Al-Balushi, M. M. Rahman, Convective heat transfer utilizing magnetic nanoparticles in the presence of a sloping magnetic field inside a square enclosure. J. Thermal Sci Eng Appl. 11(4) (2019) 041013.
[6] M. J. Uddin, M. S. Alam, M. M. Rahman, Natural convective heat transfer flow of nanofluids inside a quarter-circular enclosure using nonhomogeneous dynamic model. Arabian J Sci Eng. 42(5) (2017) 1883-1901.
[7] M. J. Uddin, M. S. Alam, N. Al-Salti, M. M. Rahman, Investigations of natural convection heat transfer in nanofluids filled horizontal semicircular-annulus using nonhomogeneous dynamic model. American J Heat Mass Transf. 3(6) (2016) 425-452.

[8] S. M. Al-Weheibi, M. M. Rahman, M. S. Alam, k. Vajravelu, Numerical simulation of natural convection heat transfer in a trapezoidal enclosure filled with nanoparticles. Int J Mech Sci. 131 (2017) 599-612.

[9] T. Islam, N. Parveen, M. F. A. Asad, Hydromagnetic natural convection heat transfer of copper-water nanofluid within a right-angled triangular cavity. Int J Thermofluid Sci Tech. 7(3) (2020) 070304.

[10] A. M. Rashad, S. Sivasankaran, M. A. Mansour, M. Bhuvaneswari, Magneto-convection of nanofluids in a lid-driven trapezoidal cavity with internal heat generation and discrete heating. Numer. Heat Transf Part A: Appl. 71(12) (2017) 1223-1234.

[11] Md. Fayz-Al-Asad, M. J. H. Munshi, Md. M. A. Sarker, Effect of fin length and location on natural convection heat transfer in a wavy cavity. Int J Thermofluid Sci Tech. 7(3) (2020) 070303.

[12] S.Yousefzadeh, H. Rajabi, N. Ghajari, M. M. Sarafraz, O. A. Akbari, M. Goodarzi, Numerical investigation of mixed convection heat transfer behavior of nanofluid in a cavity with different heat transfer areas. J. Therm Anal Calorim. 140 (2020) 2779-2803.

[13] B. Sailaja, G.S rinivas, B. S. Babu, Free and Forced Convective Heat Transfer through a Nanofluid with Two Dimensions past Stretching Vertical Plate. Int J Thermofluid Sci Tech. 7(3) (2020) 070302.

[14] H. Goodarzi, O. A. Akbari, M. M. Sarafraz, M. M. Karchegani, M. R. Safaei, G. A. Sheikh Shabani, Numerical simulation of natural convection heat transfer of nanofluid with Cu, MWCNT, and Al_2O_3 nanoparticles in a cavity with different aspect ratios. J Thermal Sci Eng Appl. 11(6) (2019) 061020.

[15] S. Kakaç, A. Pramuanjaroenkij, Review of convective heat transfer enhancement with nanofluids. Int J Heat Mass Transf. 52(13-14) (2009) 3187-3196.

[16] K. Bashirnezhad, M. M. Rashidi, Z. Yang, S. Bazri, W .M. Yan, A comprehensive review of last experimental studies on thermal conductivity of nanofluids. J Therm Analy Calori. 122(2) (2015) 863-884.

[17] D. A. Nield, A. Bejan, Convection in porous media, 4th edn. Springer, New York (2013).

[18] A. Kasaeian, R. Daneshazarian, O. Mahian, L. Kolsi, A. J. Chamkha, S. Wongwises, I. Pop, Nanofluid flow and heat transfer in porous media: a review of the latest developments. Int. J. Heat Mas Transf. 107 (2017) 778-79.

[19] M. M. Rashidi, A. Basiriparsa, L. Shamekhi, E. Momoniat, Entropy generation analysis of the revised Cheng-Minkowycz problem for natural convective boundary layer flow of nanofluid in a porous medium. Thermal Sci. 19 (2015) 169-178.

[20] M. M. Rahman, I. Pop, M. Z. Saghir, Steady free convection flow within a titled nanofluid saturated porous cavity in the presence of a sloping magnetic field energized by an exothermic chemical reaction administered by Arrhenius kinetics. Int J Heat Mas Transf. 129 (2019) 198-211.

[21] Z. Li, F. Selimefendigil, M. Sheikholeslami, A. Shafee, M. Alghamdi, Hydrothermal analysis of nanoparticles transportation through a porous compound cavity utilizing two temperature model and radiation heat transfer under the effects of magnetic field. Microsys Tech. 26(2) (2020) 333-344.

[22] F. Wu, G. Wang, W. Zhou, A thermal nonequilibrium approach to natural convection in a square enclosure due to the partially cooled sidewalls of the enclosure. Numer Heat Transf Part A: Appl. 67(7) (2015) 771-790.

[23] C. G. Mohan, A. Satheesh, The numerical simulation of double-diffusive mixed convection flow in a lid-driven porous cavity with magnetohydrodynamic effect. Arabian J Sci Eng. 41(5) (2016) 1867-1882.

[24] A. M. Rashad, R .S. R. Gorla, M. A. Mansour, S. E. Ahmed, Magnetohydrodynamic effect on natural convection in a cavity filled with a porous medium saturated with nanofluid. J Porous Media. 20(4) (2017) 363-379.

[25] A. M. Rashad, M. M. Rashidi, G. Lorenzini, S. E. Ahmed, A. M. Aly, Magnetic field and internal heat generation effects on the free convection in a rectangular cavity filled with a porous medium saturated with Cu–water nanofluid. Int J Heat Mass Transf. 104 (2017) 878-889.

[26] A. Chamkha, A. M. Rashad, T. Armaghani, M. A. Mansour, Effects of partial slip on entropy generation and MHD combined convection in a lid-driven porous enclosure saturated with a Cu–water nanofluid. J Therm Analy Calori. 132(2) (2018) 1291-1306.

[27] K. S. Al-Kalbani, M. M. Rahman, M. Z. Saghir, Entropy generation in hydromagnetic nanofluids flow inside a tilted square enclosure under local thermal nonequilibrium conditions. Int J Thermofluids (2020) doi.org/10.1016/j.ijft.2020.1000.

[28] T. Basak, S. Roy, A. J. Chamkha, A Peclet number based analysis of mixed convection for lid-driven porous square cavities with various heating of bottom wall. Int Commun Heat Mass Transf. 39(5) (2012) 657-664.

[29] A. J. Chamkha, M. A. Ismael, Natural convection in differentially heated partially porous layered cavities filled with a nanofluid. Numer Heat Transf Part A: Appl. 65(11) (2014) 1089-1113.

[30] D. A. Nield, Modeling fluid flow in saturated porous media and at interfaces. In Transp Phenom Porous Media II. (2002) 1-19.

[31] C. Ye, B. Li, W. Sun, Quasi-steady-state and steady-state models for heat and moisture transport in textile assemblies. Proc Royal Soc A: Math Phys Eng Sci. 466 (2122) (2010) 2875-2896.

[32] B. Straughan, Tipping points in Cattaneo–Christov thermohaline convection. Proc Royal Soci A: Math Phys Eng Sci. 467(2125) (2010) 7-18.

[33] W. J. Minkowycz, A. Haji-Sheikh, K. F. Vafai, On departure from local thermal equilibrium in porous media due to a rapidly changing heat source: the Sparrow number. Int J Heat Mass Transfer. 42(18) (1999) 3373-3385.

[34] C. Wang, M. Mobedi, F. Kuwahara, Simulation of heat transfer in a closed-cell porous media under local thermal non-equilibrium condition. Int J Numer Meth Heat Fluid Flow. 29(8) (2019) 2478-2500.

[35] C. Wang, M. Mobedi, A comprehensive pore scale and volume average study on solid/liquid phase change in a porous medium. Int J Heat Mass Transfer. 159 (2020) 120102.

[36] H. Zargartalebi, M. Ghalambaz, A. Noghrehabadi, A. J. Chamkha, Natural convection of a nanofluid in an enclosure with an inclined local thermal non-equilibrium porous fin considering Buongiorno's model. Numer Heat Transfer, Part A: Appl. 70(4) (2016) 432-445.

[37] A. J. Chamkha, S. Sazegar, E. Jamesahar, M. Ghalambaz, Thermal non-equilibrium heat transfer modeling of hybrid nanofluids in a structure composed of the layers of solid and porous media and free nanofluids. Energies. 12(3) (2019) 541.

[38] S. Sivasankaran, A. I. Alsabery, I. Hashim, Internal heat generation effect on transient natural convection in a nanofluid-saturated local thermal non-equilibrium porous inclined cavity. Physica A: Stat Mech Appl. 509 (2018) 275-293.

[39] H. Zargartalebi, M. Ghalambaz, M. A. Sheremet, I. Pop, Unsteady Free Convection in a Square Porous Cavity Saturated With Nanofluid: The Case of Local Thermal Nonequilibrium and Buongiorno's Mathematical Models. J Porous Media. 20(11) (2017) 999-1016.

[40] S. A. M. Mehryan, M. Ghalambaz, A. J. Chamkha, M. Izadi, Numerical study on natural convection of Ag–MgO hybrid/water nanofluid inside a porous enclosure: A local thermal non-equilibrium model. Powder Tech. 367 (2020) 443-455.

[41] M. Ghalambaz, A. Doostani, E. Izadpanahi, A. J. Chamkha, Conjugate natural convection flow of Ag–MgO/water hybrid nanofluid in a square cavity. J Therm Anal Calorim. 139(3) (2020) 2321-2336.
[42] S. A. M. Mehryan, E. Izadpanahi, M. Ghalambaz, A. J. Chamkha, Mixed convection flow caused by an oscillating cylinder in a square cavity filled with Cu–Al_2O_3/water hybrid nanofluid. J Therm Anal Calorim. 37(3) (2019) 965-982.
[43] H. Arasteh, R. Mashayekhi, M. Goodarzi, S. H. Motaharpour, M. Dahari, D. Toghraie, Heat and fluid flow analysis of metal foam embedded in a double-layered sinusoidal heat sink under local thermal non-equilibrium condition using nanofluid. J Therm Anal Calorim. 138 (2019) 1461–1476.
[44] M. Sheikholeslami, S. A. Shehzad, Simulation of water based nanofluid convective flow inside a porous enclosure via non-equilibrium model. Int J Heat Mass Transf. 120 (2018) 1200-1212.
[45] M. S. Astanina, M. Sheremet, C. J. Umavathi, Unsteady natural convection in a partially porous cavity having a heat-generating source using local thermal non-equilibrium model. Int J Heat Fluid Flow. 29(6) (2019) 1902-1919.
[46] S. M. Al-Weheibi, M. M. Rahman, Convective heat transmission inside a porous trapezoidal enclosure occupied by nanofluids: local thermal nonequilibrium conditions for a porous medium. Italian J Eng Sci: Tec Italiana. 61+1 (2) (2018) 102-114.
[47] M. A. Sheremet, I. Pop, R. Nazar, Natural convection in a square cavity filled with a porous medium saturated with a nanofluid using the thermal nonequilibrium model with a Tiwari and Das nanofluid model. Int J Mech Sci. 100 (2015) 312-321.
[48] R. K. Tiwari, M. K. Das, Heat transfer augmentation in a two-sided lid-driven differentially heated square cavity utilizing nanofluids. Int J Heat Mass Transf. 50(9-10) (2007) 2002-2018.
[49] M. Izadi, R. Mohebbi, H. Sajjadi, A. A. Delouei, LTNE modeling of Magneto-Ferro natural convection inside a porous enclosure exposed to nonuniform magnetic field. Physica A: Statis Mech Appl. 535 (2019) 122394.
[50] M. Ghalambaz, A. Tahmasebi, A. J. Chamkha, D. Wen, Conjugate local thermal non-equilibrium heat transfer in a cavity filled with a porous medium: Analysis of the element location. Int J Heat Mass Transf. 138 (2019) 941-960.
[51] M. Sabour, M. Ghalambaz, Natural convection in a triangular cavity filled with a nanofluid-saturated porous medium using three heat equation model. Canadian J Phys. 94(6) (2016) 604-615.
[52] I. Pop, M. Ghalambaz, M. Sheremet, Free convection in a square porous cavity filled with a nanofluid using thermal non equilibrium and Buongiorno models. Int J Heat Fluid Flow. 26(3/4) (2016) 671-693.
[53] S. M. Al-Weheibi, M. M. Rahman, M. Z. Saghir MZ Impacts of variable porosity and variable permeability on the thermal augmentation of Cu-H_2O nanofluid drenched porous trapezoidal enclosure considering thermal nonequilibrium model. Arabian J Sci Eng. 45(2) (2020) 1237-1251.
[54] S. Abelman, A. B. Parsa, H. O. Sayehvand, Nanofluid flow and heat transfer in a Brinkman porous channel with variable porosity. Quaes Mathemat 41(4) (2018) 449-467.
[55] H. C. Brinkman, A calculation of the viscous force exerted by a flowing fluid on a dense swarm of particles. Flow Turbu Combus. 1(1) (1949) 27-34.
[56] H. C. Brinkman, On the permeability of media consisting of closely packed porous particles. Flow Turbu Combus. 1(1) (1949) 81-86.
[57] J. A. Ochoa-Tapia, S. Whitaker, Momentum transfer at the boundary between a porous medium and a homogeneous fluid—II. Comparison with experiment. Int J Heat Mass Transf. 8(14) (1995) 2647-2655.
[58] B. C. Chandrasekhara, D. Vortmeyer, Flow model for velocity distribution in fixed porous beds under isothermal conditions. Wärme-und Stoffübertragung. 12(2) (1979) 105-111.

[59] C. T. Hsu, P. Cheng, Closure schemes of the macroscopic energy equation for convective heat transfer in porous media. International Commun Heat Mass Transf. 15(5) (1988) 689-703.
[60] S. Ergun, Fluid Flow through Packed Columns. Chem Eng Sci. 48 (2) (1952) 89-94.
[61] H. C. Brinkman, The viscosity of concentrated suspensions and solutions. The J Chem Phys. 20(4) (1952) 571-571.
[62] J. C. Maxwell, A treatise on electricity and magnetism, Vol I, II. Clarendon Press, Oxford (1873).
[63] H. F. Oztop, E. Abu-Nada, Numerical study of natural convection in partially heated rectangular enclosures filled with nanofluids. Int J Heat Fluid Flow. 29(5) (2008) 1326-1336.
[64] H. T. Cheohg, S. Sivasankaran, Z. Siri, Effect of wall inclination on natural convection in a porous trapezoidal cavity. AIP Conference Proceedings 1605, 343 (2014) doi.org/10.1063/1.4887613.
[65] K. S. Al-Kalbani, M. S. Alam, M. M. Rahman, Finite element analysis of unsteady natural convective heat transfer and fluid flow of nanofluids inside a tilted square enclosure in the presence of oriented magnetic field. American J Heat Mass Transf. 3 (2016) 186–224.
[66] M. J. Uddin, M. M. Rahman, Numerical computation of natural convective heat transport within nanofluids filled semi-circular shaped enclosure using nonhomogeneous dynamic model. Thermal Sci Eng Prog. 1(2017) 25-38.
[67] O. C. Zienkiewicz, R. L. Taylor, The finite element method, Vol. 36. McGraw-Hill., London (1977).
[68] A. C. Baytas, I. Pop, Free convection in oblique enclosures filled with a porous medium. Int J Heat Mass Transfer. 42 (1999) 1047–1057.